A Global Survey of Static Stability in the Stratosphere and Upper Troposphere

KEVIN M. GRISE, DAVID W. J. THOMPSON, AND THOMAS BIRNER

Department of Atmospheric Science, Colorado State University, Fort Collins, Colorado

(Manuscript received 4 August 2009, in final form 7 December 2009)

ABSTRACT

Static stability is a fundamental dynamical quantity that measures the vertical temperature stratification of the atmosphere. However, the magnitude and structure of finescale features in this field are difficult to discern in temperature data with low vertical resolution. In this study, the authors apply more than six years of high vertical resolution global positioning system radio occultation temperature profiles to document the long-term mean structure and variability of the global static stability field in the stratosphere and upper troposphere.

The most pronounced feature in the long-term mean static stability field is the well-known transition from low values in the troposphere to high values in the stratosphere. Superposed on this general structure are a series of finer-scale features: a minimum in static stability in the tropical upper troposphere, a broad band of high static stability in the tropical stratosphere, increases in static stability within the core of the stratospheric polar vortices, and a shallow but pronounced maximum in static stability just above the tropopause at all latitudes [i.e., the ''tropopause inversion layer'' (TIL)].

The results shown here provide the first global survey of static stability using high vertical resolution data and also uncover two novel aspects of the static stability field. In the tropical lower stratosphere, the results reveal a unique vertically and horizontally varying static stability structure, with maxima located at ~17 and ~19 km. The upper feature peaks during the NH cold season and has its largest magnitude between 10° and 15° latitude in both hemispheres; the lower feature exhibits a weaker seasonal cycle and is centered at the equator. The results also demonstrate that the strength of the TIL is closely tied to stratospheric dynamic variability. The magnitude of the TIL is enhanced following sudden stratospheric warmings in the polar regions and the easterly phase of the quasi-biennial oscillation in the tropics.

1. Introduction

The vertical temperature stratification of the atmosphere, or static stability, plays a fundamental role in all scales of atmospheric motions. Static stability is often defined as the square of the buoyancy frequency N, which measures the frequency of the vertical oscillation of an air parcel that is displaced adiabatically from an equilibrium state in a stably stratified atmosphere (e.g., Andrews et al. 1987). Because buoyancy is the dominant restoring force for vertical motions in the atmosphere, static stability is central to the dispersion relations for atmospheric waves, such as gravity waves, Kelvin waves, and Rossby waves. Consequently, an accurate understanding of atmospheric wave propagation requires precise knowledge of the vertical and horizontal structure of static stability.

Finescale features in the atmospheric static stability field are often neglected in theoretical studies, including those that apply the quasigeostrophic refractive index (e.g., Andrews et al. 1987). Arguments based upon quasigeostrophic theory define static stability from a reference state potential temperature profile that is a function of height only. The few theoretical studies that have accounted for finescale vertical gradients in the quasigeostrophic reference state have demonstrated that such structures can have a profound effect on stationary Rossby waves (Lindzen 1994; see also correction in Lindzen and Roe 1997). Hence, the nature of the horizontal, vertical, and temporal variability of the static stability field could be important for unlocking the physics behind complicated problems in atmospheric dynamics, such as recent observations of coupling between extratropical stratospheric and tropospheric flow (e.g., Baldwin and Dunkerton 2001) that are inextricably linked to atmospheric wave processes.

The structure of the static stability field below ~50 km is dominated by the tropopause, which serves as a sharp transition between lower values of static stability in the

Corresponding author address: Kevin M. Grise, Dept. of Atmospheric Science, Colorado State University, 1371 Campus Delivery, Fort Collins, CO 80523.
E-mail: kgrise@atmos.colostate.edu

DOI: 10.1175/2009JCLI3369.1

troposphere ($N^2 \approx 1.0 \times 10^{-4}$ s^{-2}) and higher values of static stability in the stratosphere ($N^2 \approx 5.0 \times 10^{-4}$ s^{-2}). Theoretical studies have demonstrated that the long-term mean height of the tropopause reflects a balance between radiative and dynamical processes (e.g., Held 1982). The dynamical processes are governed primarily by moist convection in the tropics and by both tropospheric baroclinic eddies (e.g., Held 1982; Haynes et al. 2001; Schneider 2004) and moist convection (Juckes 2000; Frierson et al. 2006; Frierson 2008) in the extratropics. The seasonal cycle and intraseasonal variability in the height of the tropopause are similarly influenced by a variety of factors. In the tropics, variability in the height of the tropopause has been linked to the strength of the Brewer–Dobson circulation (e.g., Yulaeva et al. 1994; Highwood and Hoskins 1998; Gettelman and Forster 2002), the quasi-biennial oscillation (QBO; e.g., Randel et al. 2000; Zhou et al. 2001), and convectively coupled equatorial wave activity (e.g., Ryu et al. 2008; Fueglistaler et al. 2009). In the extratropics, variability in the height of the tropopause has been linked to polar stratospheric dynamical heating (Zängl and Hoinka 2001), eddy heat fluxes (Son et al. 2007), and the sign of tropospheric relative vorticity (e.g., Zängl and Wirth 2002).

The availability of high vertical resolution datasets has allowed more recent studies to focus not only on the height of the tropopause but also on the vertical gradient in static stability across it. Using high vertical resolution radiosonde data, Birner et al. (2002) and Birner (2006) identified a region of enhanced static stability in a shallow layer directly above the extratropical tropopause. The region of enhanced static stability, referred to as the tropopause inversion layer (TIL), had not been widely recognized in prior literature because 1) averaging with respect to a tropopause-relative vertical coordinate makes it easier to distinguish the TIL (Birner et al. 2002) and 2) the TIL tends to be smeared out in reanalysis products based on data assimilation (Birner et al. 2006). More recent studies have examined characteristics of the TIL using global positioning system (GPS) radio occultation temperature profiles (Randel et al. 2007b), the interpolation of conventional radiosonde data (Bell and Geller 2008), and idealized general circulation model experiments (Son and Polvani 2007).

The physical explanation for the existence of the TIL is still subject to debate. Randel et al. (2007b) hypothesized that the TIL is radiatively driven because, in the lower stratosphere, radiative heating due to ozone dominates in a layer just above where radiative cooling due to water vapor is important. In contrast, Wirth (2003) proposed that the climatological TIL is dynamically driven. Wirth (2003) argued that 1) anticyclonic systems are associated with stronger static stability than cyclonic systems near the tropopause level and 2) anticyclonic systems dominate the zonal average because the static stability anomaly in anticyclonic systems is much stronger and sharper than the static stability anomaly in comparable cyclonic systems. Wirth and Szabo (2007) have subsequently argued that the vertical velocity convergence associated with the formation of anticyclonic systems is responsible for the TIL. However, the vertical velocity convergence associated with the stratospheric residual circulation may also play an important role in forcing the TIL at midlatitudes during winter (Birner 2010).

In this paper, we present the first global survey of static stability in the stratosphere and upper troposphere as a function of latitude, longitude, and season using high vertical resolution temperature data. We also document for the first time the relationship between stratospheric processes and the magnitude of near-tropopause static stability (i.e., the TIL) at tropical and polar latitudes. The results support previous analyses of static stability and also provide several novel insights into both the long-term mean structure and variability of the global static stability field. Section 2 describes the data and methods used in this study. The results are then centered around two themes. We first focus on the zonal-mean climatology of the global static stability field in the stratosphere and upper troposphere: section 3 examines the annual-mean, zonal-mean climatology of static stability and discusses the sensitivity of the results to the choice of vertical coordinate system; and section 4 examines the seasonal cycle of the zonal-mean static stability field. We then focus on the processes associated with spatial and temporal variability in the TIL: section 5 examines the longitudinal structure of the TIL and section 6 identifies processes linked to weekly and monthly variability in the TIL. Summarizing and concluding remarks are given in section 7.

2. Data and methods

a. Data

The primary data used in this study are the GPS radio occultation temperature profiles derived from the Challenging Minisatellite Payload (CHAMP) satellite (Wickert et al. 2001). The data are freely available from the University Corporation for Atmospheric Research (UCAR)'s Constellation Observing System for Meteorology, Ionosphere, and Climate (COSMIC) program and are provided at 100-m vertical resolution from the surface to ~40 km altitude. Over the globe, approximately 200 CHAMP profiles are available per day. The current available data record extends from 19 May 2001 to 4 October 2008, but the number of daily profiles is

much lower prior to 10 March 2002 (cf. Fig. 9 of Hajj et al. 2004). Consequently, we focus only on data for the period following 10 March 2002. The more recent COSMIC mission provides an order of magnitude increase in the number of global profiles per day (Anthes et al. 2008). However, the COSMIC data record, which begins in 2006, is too short for the purposes of this project.

The GPS temperature dataset offers the only global, high vertical resolution measurements of atmospheric temperature: select radiosondes have comparable vertical resolution but cover only a fraction of the globe; other satellite temperature products provide global coverage but have coarse vertical resolution. GPS radio occultation temperature retrievals are affected by water vapor, but the biases in the GPS data due to water vapor are very small in regions where temperatures are colder than 250 K (Kursinski et al. 1996). Here, we focus on the GPS data at levels above the upper troposphere where water vapor is known to have little effect on the GPS temperature retrievals (e.g., Kursinski et al. 1996).

To help interpret several features in the static stability field, we supplement the GPS temperature profiles with zonal winds and geopotential heights from the National Centers for Environmental Prediction–National Center for Atmospheric Research (NCEP–NCAR) reanalysis dataset (Kalnay et al. 1996). The reanalysis data are obtained from the Physical Sciences Division of the National Oceanic and Atmospheric Administration's Earth System Research Laboratory and are truncated to the period following 1979 when more comprehensive satellite data are included in the reanalysis data assimilation scheme (Kalnay et al. 1996; Kistler et al. 2001).

b. Methods

Static stability is defined throughout this study using (1), where g is 9.81 m s^{-2} and θ is potential temperature:

$$N^2 = \frac{g}{\theta}\frac{\partial\theta}{\partial z}. \quad (1)$$

The height of the tropopause is identified using thermal criteria. The thermal tropopause is defined as the lowest level at which 1) the atmospheric lapse rate is 2 K km^{-1} or less and 2) does not exceed 2 K km^{-1} between that level and all higher levels within 2 km (WMO 1957).

The results of this study are calculated in both a conventional vertical coordinate system (i.e., fixed altitude) and a tropopause-relative vertical coordinate system (e.g., Birner et al. 2002; Birner 2006). In the case of tropopause-relative coordinates, all GPS temperature profiles are shifted vertically so that the thermal tropopause for all profiles is located at a fixed value on the ordinate axis. The premise behind tropopause-relative coordinates is that the height of the tropopause fluctuates as a function of time and space, so finescale features near the tropopause are masked in long-term averages based on conventional altitude or pressure coordinate systems. Note that because the thermal tropopause is not easily detected during winter over Antarctica (e.g., Zängl and Hoinka 2001), results using tropopause-relative coordinates are difficult to interpret there (Tomikawa et al. 2009).

To characterize intraseasonal dynamic variability in the Northern Hemisphere (NH) extratropical stratospheric flow, we use the standardized leading principal component (PC) time series of the NCEP–NCAR reanalysis daily-mean 10-hPa geopotential height anomalies calculated for the months of November–April between 1979 and 2008 and for the region 20°–90°N. The geopotential height anomalies were detrended and scaled by the square root of the cosine of the latitude prior to calculating the PC time series. The resulting PC time series describes intraseasonal variability in the strength of the stratospheric polar vortex and is referred to herein as the northern annular mode (NAM) index at 10 hPa. By definition, positive values of the 10-hPa NAM index are associated with stronger-than-normal flow along 60°N, and negative values of the 10-hPa NAM index are associated with an anomalously weak stratospheric polar vortex (see also Baldwin and Dunkerton 2001). Hence, large negative values of the 10-hPa NAM index are linked to sudden stratospheric warmings. We note that the results based on the 10-hPa NAM index are not sensitive to changes in the index used to characterize stratospheric variability; virtually identical results are derived from an index based on the 10-hPa zonal-mean zonal wind at 60°N.

To characterize temporal variability in the QBO, a QBO index time series is defined using the standardized 1979–2008 NCEP–NCAR reanalysis daily-mean, zonal-mean 50-hPa zonal wind anomalies averaged over the region 20°N–20°S. The zonal wind anomalies were detrended prior to calculating the QBO index time series. By definition, the QBO index time series is positive (negative) when the 50-hPa zonal wind in the tropics is westerly (easterly).

The statistical significance of the regression coefficient between two time series is estimated by testing whether the associated correlation coefficient is significantly different from zero. The testing is performed using a Student's t statistic applied to the correlation coefficient r with $n^* - 2$ degrees of freedom:

$$t = r\sqrt{\frac{n^* - 2}{1 - r^2}}. \quad (2)$$

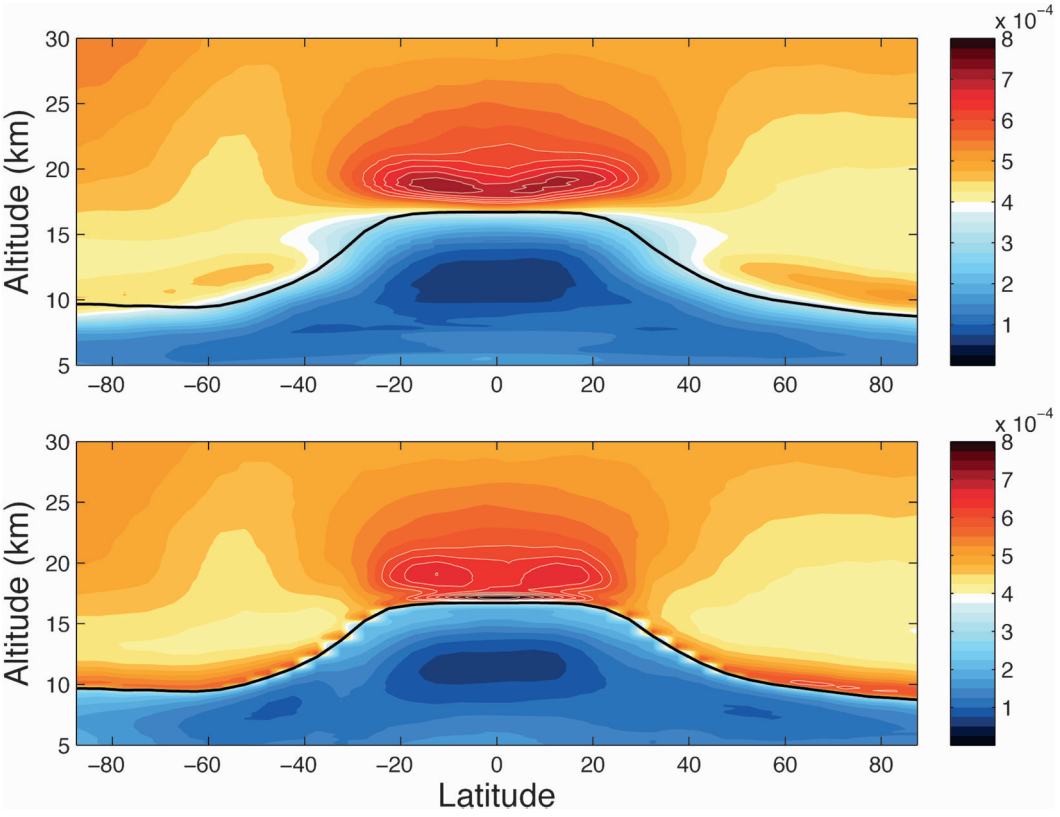

FIG. 1. Annual-mean, zonal-mean static stability (N^2) in (top) conventional vertical coordinates and (bottom) tropopause-relative vertical coordinates. The shading interval is 2.5×10^{-5} s^{-2}. The thick solid black line is the annual-mean, zonal-mean thermal tropopause height. The thin white contours highlight the shading intervals for values greater than or equal to 6.0×10^{-4} s^{-2}. The annual mean is based on data averaged over April 2002–March 2008. In all figures, static stability is calculated using the GPS temperature profiles from the CHAMP satellite.

The effective sample size n^* is estimated using the relation

$$n^* = n\frac{1 - r_1 r_2}{1 + r_1 r_2}, \tag{3}$$

where n is the number of samples and r_i is the lag-1 autocorrelation for the time series i (Bretherton et al. 1999).

3. The annual-mean, zonal-mean static stability field

In this section, we document the annual-mean, zonal-mean structure of static stability in the stratosphere and upper troposphere. The results are examined using both conventional vertical coordinates and tropopause-relative vertical coordinates.

a. Conventional vertical coordinates

The top panel in Fig. 1 shows annual-mean, zonal-mean values of static stability in the stratosphere and upper troposphere using altitude as the vertical coordinate. The solid black line represents the annual-mean, zonal-mean height of the thermal tropopause.

The most prominent feature in the global static stability field is the abrupt vertical transition between tropospheric values ($N^2 \approx 1.0 \times 10^{-4}$ s^{-2}) and stratospheric values ($N^2 \approx 5.0 \times 10^{-4}$ s^{-2}) (e.g., Peixoto and Oort 1992). In the extratropics, this feature is superposed by a shallow local maximum located approximately 1–2 km above the tropopause. The local maximum represents the signature of the TIL in conventional vertical coordinates (Birner 2006). In the annual mean, the strength of the TIL is larger at NH high latitudes than it is at SH high latitudes because of the virtual disappearance of the TIL during SH polar winter (e.g., Tomikawa et al. 2009). (The seasonal cycle of the TIL is discussed in section 4.) The extratropical static stability decreases rapidly with height just above the TIL and then slowly increases with height through the midstratosphere.

In the tropics, the annual-mean static stability field is characterized by three principal features: a minimum in

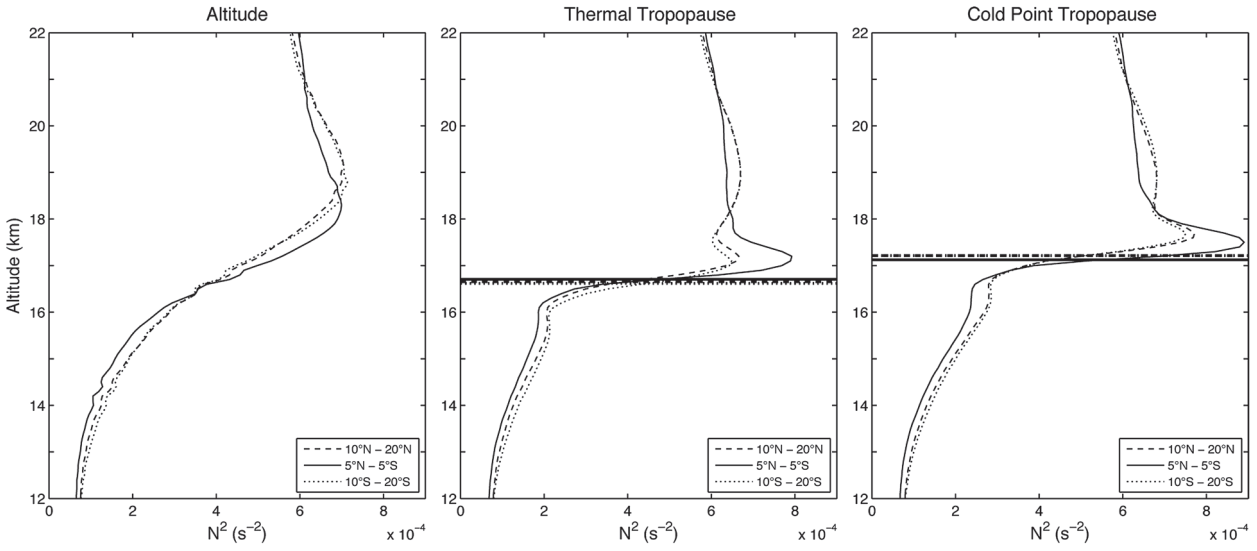

FIG. 2. Vertical profiles of annual-mean N^2 averaged over the latitude bands indicated in (left) conventional vertical coordinates, (middle) tropopause-relative vertical coordinates, and (right) vertical coordinates averaged with respect to the cold point tropopause. The thick horizontal lines denote the annual-mean (middle) thermal tropopause heights and (right) cold point tropopause heights for the respective latitude bands.

the upper troposphere, paired off-equatorial maxima immediately above the tropopause, and a broad region of high static stability values throughout the lower and midstratosphere. In contrast to the extratropics, the static stability in the tropics decreases monotonically with height above the near-tropopause maxima. Several of the features in the tropical static stability field have long been established: the minimum in the tropical upper troposphere reflects the level at which tropospheric temperatures depart from the moist adiabatic lapse rate (e.g., Gettelman and Forster 2002; Fueglistaler et al. 2009), and the high values of static stability throughout the tropical stratosphere reflect the effects of radiative heating due to ozone (e.g., Kiehl and Solomon 1986; Andrews et al. 1987; Fueglistaler et al. 2009). But the robustness of the shallow maxima in static stability immediately above the tropopause has not been established. As demonstrated in this study, the paired shallow maxima in static stability above the tropical tropopause appear to be a ubiquitous feature of the tropical atmosphere (Fig. 1, top).

b. Tropopause-relative vertical coordinates

The bottom panel of Fig. 1 shows the same results as those in the top panel of Fig. 1, but for tropopause-relative vertical coordinates. The dominant features in the global static stability field are reproducible in both coordinate systems, including the static stability minimum in the tropical upper troposphere, the paired shallow static stability maxima in the lowermost tropical stratosphere, and the increase in static stability with height in the extratropical midstratosphere. The TIL is clearly evident in both coordinate systems in the extratropics, but it is generally shallower and stronger in tropopause-relative coordinates (see also Birner 2006).

The most notable differences between the two coordinate systems are found in association with the TIL in the subtropics and the tropics. In the subtropics, the tropopause fluctuates between tropical and extratropical characteristics, and at certain times, the subtropics are characterized by two tropopauses (Seidel and Randel 2007). There is a hint of the TIL in the subtropics in the bottom panel of Fig. 1, but the occasional presence of two tropopauses in this region renders results based on tropopause-relative coordinates difficult to interpret there.

In the tropics, the results based on tropopause-relative coordinates reveal that the tropical TIL exhibits a unique horizontally and vertically varying structure. As observed in conventional vertical coordinates, paired off-equatorial maxima in static stability are centered ~2 km above the tropopause between 10° and 15° latitude. However, in tropopause-relative coordinates, the paired maxima are accompanied by a very narrow maximum in static stability that is centered at the equator less than 1 km above the tropopause. The unique structure of the tropical TIL is even more striking in vertical profiles of static stability averaged over the 10°–20°N, 5°N–5°S, and 10°–20°S latitude bands (Fig. 2, middle). Near the equator, static stability increases rapidly above the tropopause and decreases monotonically above ~17 km. Between 10° and 20° latitude in both hemispheres, static stability also increases immediately above the tropopause (~17 km)

but exhibits a second maximum at ~19 km. The meridional and vertical structure of the tropical TIL shown in Fig. 2 (middle panel) is also evident if we use the cold point tropopause (i.e., the minimum in temperature in the upper troposphere and lower stratosphere) instead of the thermal tropopause to define tropopause-relative coordinates (Fig. 2, right); however, the shallow maximum at ~17 km is not apparent in a conventional (i.e., fixed altitude) vertical coordinate system, since the height of the tropopause fluctuates in time and space (Fig. 2, left). As evidenced in the middle and right panels of Fig. 2, the details of the shallow static stability maximum at ~17 km change slightly depending on the definition of the tropopause used to define tropopause-relative coordinates. However, the differences are minor and have no bearing on the conclusions of this study. For this reason, we use only the thermal tropopause to define tropopause-relative coordinates throughout this paper.

Figure 1 establishes that both conventional and tropopause-relative vertical coordinates are capable of capturing key features in the long-term mean static stability field, including finescale features such as the TIL. However, Fig. 1 also reveals that finescale features near the tropopause are accentuated in the tropopause-relative framework, particularly the magnitude of the extratropical TIL and the detailed structure of the tropical TIL. For this reason, the remainder of this paper focuses on results based on the tropopause-relative coordinate system.

4. The seasonal cycle in the zonal-mean static stability field

Figure 3 shows meridional cross sections of zonal-mean static stability in tropopause-relative coordinates as a function of season. The black contours show the corresponding seasonal means of the zonal-mean zonal wind. Overall, the most pronounced features in the seasonal cycle of zonal-mean static stability include the following:

1) In the polar lower stratosphere, the TIL is strongest during the summer season in both hemispheres (see also Birner 2006; Randel et al. 2007b).
2) In the polar midstratosphere, static stability peaks on the poleward flanks of the stratospheric polar night jets, particularly in the SH.
3) In the midlatitude lower stratosphere, the TIL is deepest and most clearly defined during the winter season (see also Bell and Geller 2008).
4) In the tropical lower stratosphere, the largest values of static stability occur during the NH cold season.

These four features are evident in Fig. 3 but are more readily apparent by dividing the data into latitude bands with similar static stability characteristics. In the remainder of this section, we explore these and other aspects of the seasonal cycle of zonal-mean static stability by focusing on three distinct latitude bands: polar regions (60°–90° latitude), midlatitudes (40°–60° latitude), and tropics (equatorward of 20° latitude). Our discussion begins with the polar regions.

a. Polar regions

The top row in Fig. 4 depicts the seasonal cycle of static stability in the NH (left) and SH (right) polar regions as a function of calendar month and altitude. Note that the abscissa is extended to 18 months so that the seasonal cycle is not truncated at the edges of the figure. The dashed line in each panel signifies the altitude of the maximum zonal-mean zonal flow within the 50°–75° latitude band.

As documented in Birner (2006) and Randel et al. (2007b), the high-latitude TIL is deepest and weakest during winter but shallowest and strongest during summer. The seasonal contrast is larger in the SH, where the TIL is nearly undetectable from July through October (see also Tomikawa et al. 2009). In both hemispheres, static stability in the polar upper troposphere is lowest during periods when static stability in the TIL is highest.

Interestingly, the tropopause exhibits a markedly different seasonal cycle in the two polar regions. In the NH polar regions, the tropopause (solid black line) is highest in summer when the TIL is strongest but lowest in winter when the TIL is weakest. In contrast, in the SH polar regions, the tropopause is lowest in summer when the TIL is strongest but highest in winter when the TIL is weakest. The out-of-phase seasonal cycles of the NH and SH polar thermal tropopauses are consistent with the climatology of the NH and SH polar dynamical (i.e., potential vorticity) tropopauses documented in Zängl and Hoinka (2001).

→

FIG. 3. Zonal-mean N^2 (shading) averaged over the seasons indicated using data from March 2002 to August 2008. The shading interval is 2.5×10^{-5} s^{-2}. Thin black contours denote the corresponding seasonal-mean values of the zonal-mean zonal wind from the NCEP–NCAR reanalysis (lowest contour is 20 m s^{-1}; contour interval is 10 m s^{-1}). The thick solid black line in all panels denotes the seasonal-mean, zonal-mean tropopause height. The thin white contours highlight the shading intervals for values greater than or equal to 6.0×10^{-4} s^{-2}. Results in this figure and all subsequent figures are shown in tropopause-relative coordinates.

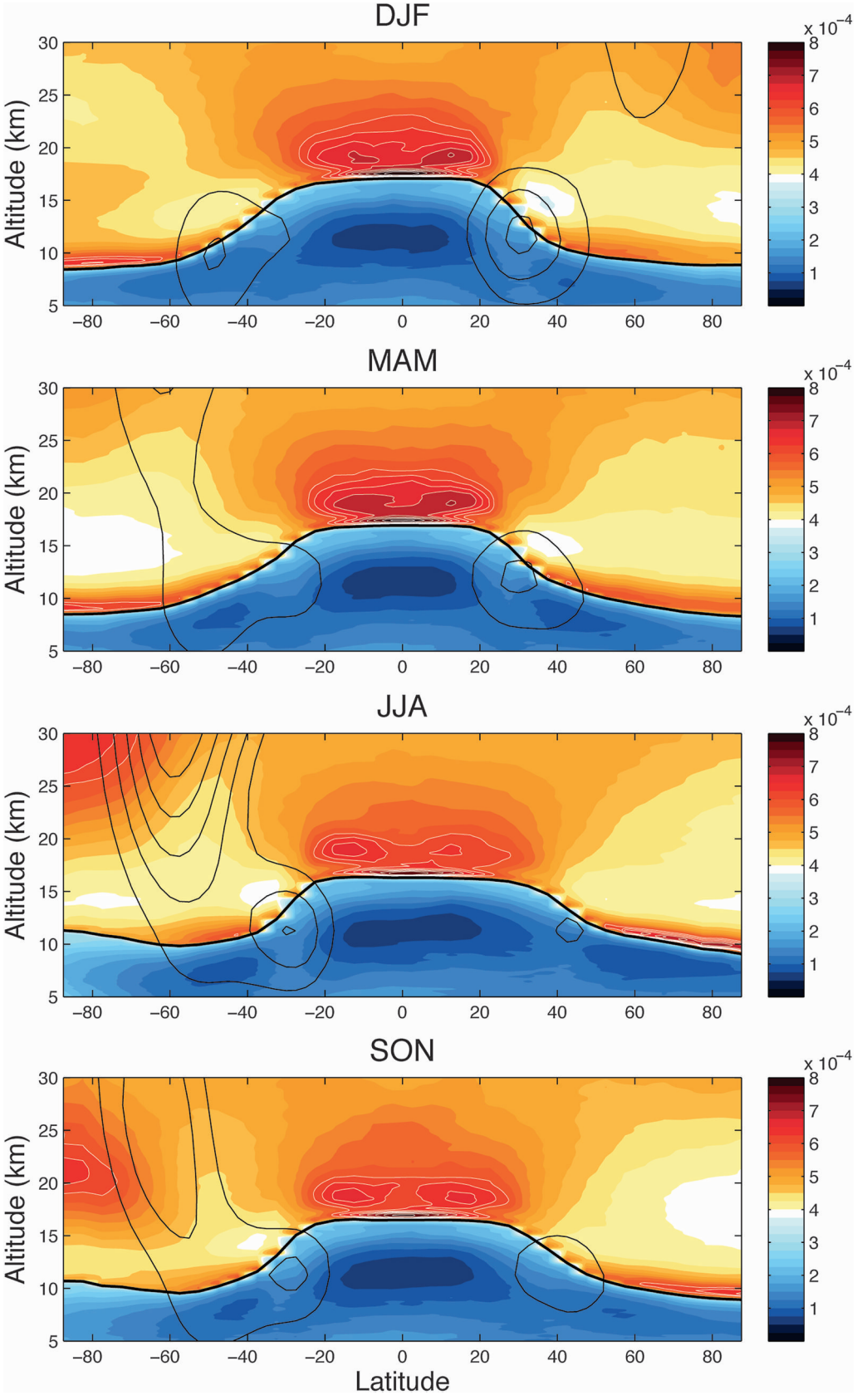
DJF
MAM
JJA
SON
Altitude (km)
Latitude
x 10^-4
30
25
20
15
10
5
−80
−60
−40
−20
0
20
40
60
80
8
7
6
5
4
3
2
1

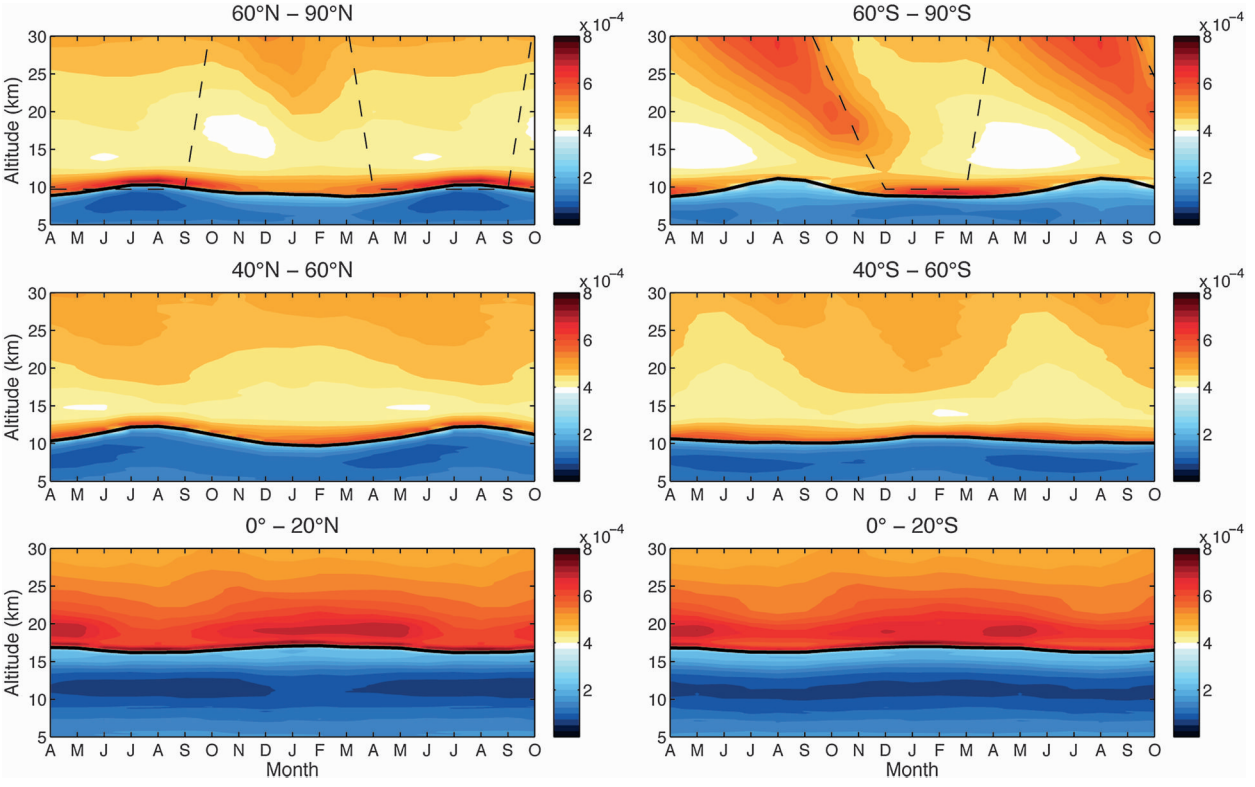

FIG. 4. Month–height plots of the seasonal cycle in N^2 for the latitude bands indicated. The shading interval is 2.5×10^{-5} s^{-2}. The thick solid black line denotes the monthly-mean tropopause height in each plot. (top) The dashed line denotes the altitude of the maximum westerly zonal wind over the latitude band 50°–75°. Note that half of the seasonal cycle is repeated in each plot so that the seasonal cycle is not truncated at the edges of the figure.

In the polar midstratosphere, the static stability is significantly larger during the cold season, particularly in the SH. The large meridional gradients in static stability in the polar midstratosphere (Fig. 3) are consistent with the requirements of thermal wind balance on the poleward flank of the westerly stratospheric polar night jet. (See the appendix for a brief description of the relationship between zonal-mean static stability and the zonal-mean zonal flow). Relative to the NH, the larger meridional gradients in static stability in the SH midstratosphere are consistent with the greater vertical curvature of the zonal wind profile associated with the SH stratospheric polar vortex (not shown). The descending of the region of peak static stability in the SH polar stratosphere corresponds to the seasonal breakdown of the SH stratospheric polar vortex (e.g., Hartmann 1976); as noted in section 6, a similar (but opposite in sign) signal in static stability is found in association with sudden stratospheric warmings.

b. *Midlatitudes*

The middle row in Fig. 4 documents the seasonal cycle of static stability averaged over the NH (left) and SH (right) midlatitudes. In contrast to the polar regions, the TIL exhibits a weak seasonal cycle when averaged over the 40°–60° latitude band (see also Randel et al. 2007b). The reasons for the weak seasonal cycle in Fig. 4 (middle row) are evidenced in Fig. 3. During the winter season, the midlatitude TIL is relatively weak but extends throughout the 40°–60° latitude band. In contrast, during the summer season, the TIL has large amplitude on the poleward edge of the 40°–60° latitude band but is poorly defined on the equatorward edge of the 40°–60° latitude band. Hence, when averaged over the midlatitudes, the summertime and wintertime magnitudes of the TIL are comparable.

In the midlatitude midstratosphere, the static stability is strongest during the summer season, again in contrast to the seasonal cycle in the polar regions. The seasonal cycle in static stability in the midlatitude midstratosphere is consistent with 1) the extension of the region of high static stability from the tropics into the midlatitudes during summer (Fig. 3), 2) the enhanced radiative heating due to ozone in the midlatitude stratosphere during summer (e.g., Kiehl and Solomon 1986; Andrews et al. 1987), and 3) the requirements of thermal wind balance on the equatorward flank of the westerly stratospheric polar night jet during winter (see the appendix).

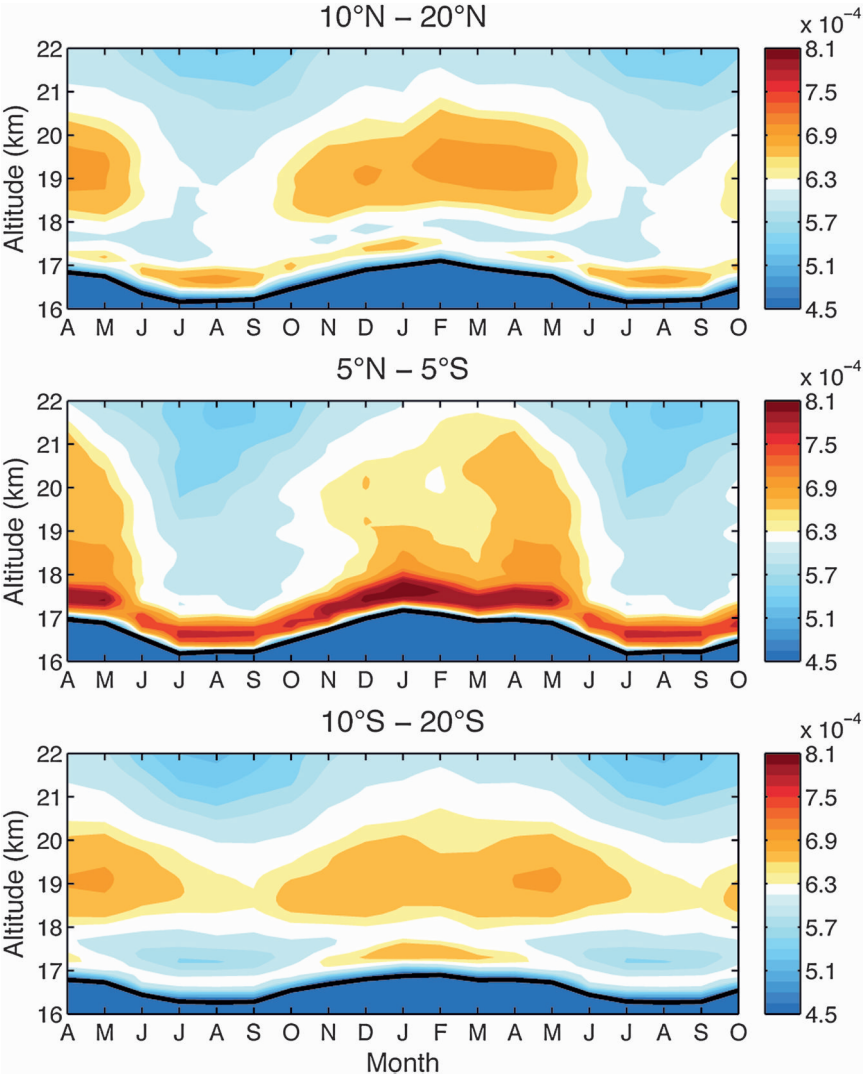

FIG. 5. As in Fig. 4, but for results averaged over select tropical latitude bands and focused on the tropical tropopause region. The shading interval is 1.5×10^{-5} s^{-2}, with values below 4.5×10^{-4} s^{-2} not contoured. The thick solid black line is the monthly-mean tropopause height in each plot. Note that the shading interval has been changed from Fig. 4 to emphasize the vertical structure of the tropical features.

c. *Tropics*

The bottom row in Fig. 4 displays the seasonal cycle of static stability in the NH (left) and SH (right) tropics. As noted in section 3, the most interesting features in static stability in the tropics are found in the vicinity of the tropopause. Hence, in Fig. 5, we reproduce the results from the bottom row of Fig. 4, but we focus on the region between 16 and 22 km. To demonstrate the meridional structure of the tropical features, Fig. 5 divides the tropics into three latitude bands in which unique static stability structures are evident in the annual mean (see Figs. 1 and 2): 10°–20°N (top panel), 5°N–5°S (middle panel), and 10°–20°S (bottom panel). Note that the color bar in Fig. 5 is different than that in Fig. 4 so that the finescale features near the tropopause are accentuated.

Figure 5 confirms the existence of two distinct features in the tropical TIL: a narrow maximum centered at ~17 km and a broader maximum centered at ~19 km. The narrow static stability maximum centered at ~17 km is strongest in the 5°N–5°S latitude band (Fig. 5, middle) and weakly peaks during NH winter. The narrow maximum is weaker in the 10°–20° latitude bands and peaks during the summer season. The broader static stability maximum near 19 km is more distinct poleward of 10° latitude and peaks during the NH cold season in both

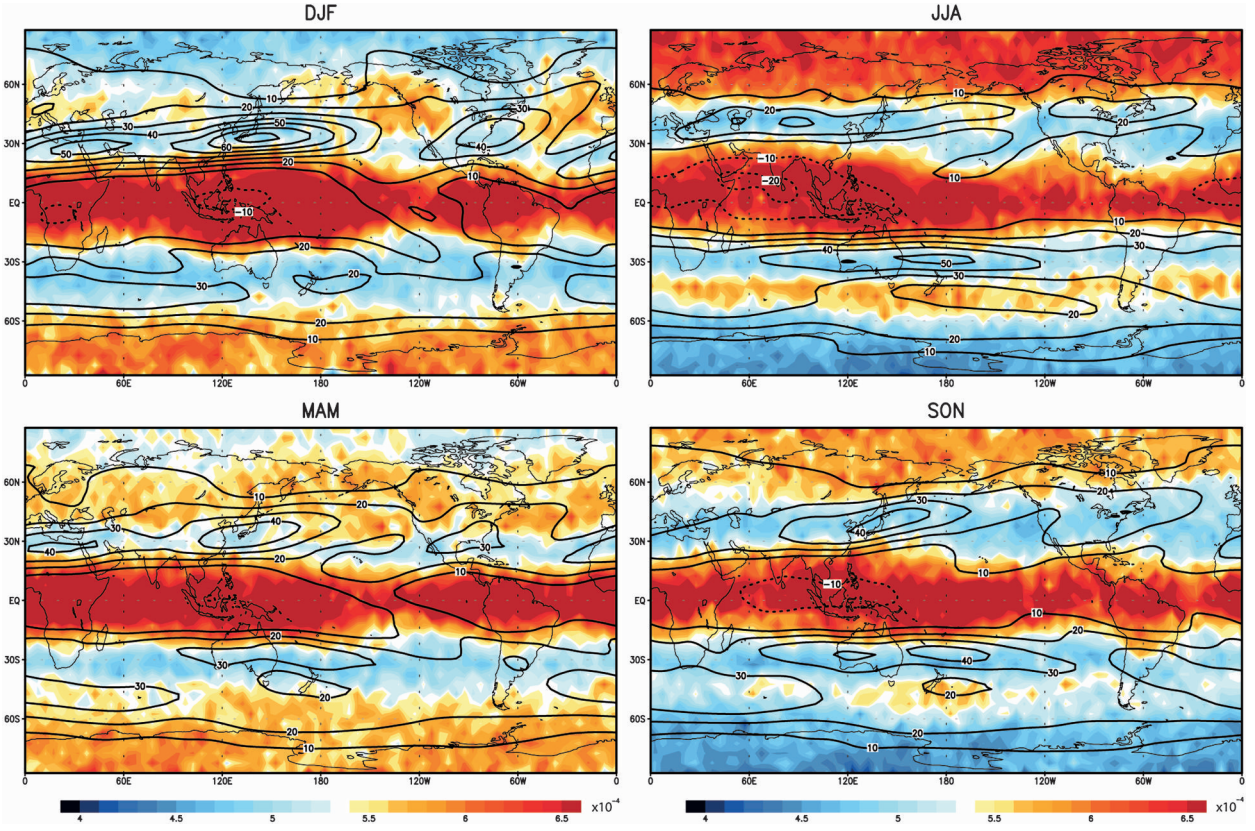

FIG. 6. Static stability averaged over the 0–1-km layer above the tropopause (shading) for the seasons indicated. The black contours denote the 200-hPa zonal wind from the NCEP–NCAR reanalysis. The shading interval is 1.0×10^{-5} s^{-2}, with values above 6.5×10^{-4} s^{-2} not contoured. The contour interval for the 200-hPa zonal wind is 10 m s^{-1}. Positive contours are solid, negative contours are dashed, and the zero contour has been omitted.

hemispheres. The seasonal cycle in static stability at 19 km is consistent with the large amplitude of the seasonal cycles in temperature and ozone over the 16–19-km altitude range (Randel et al. 2007a). But to our knowledge, the existence of the equatorially centered feature near 17 km has not been previously documented. We examine both features in further detail in the next section.

5. Longitudinal structure of near-tropopause static stability

In this section and the next section, we focus on the zonally and temporally varying aspects of the region of enhanced static stability immediately above the tropopause (i.e., the TIL). We focus on this region for several reasons. First, the structure of static stability in the midstratosphere has been extensively documented and is consistent with 1) stratospheric radiative heating rates (e.g., Kiehl and Solomon 1986) and 2) the collocation of large temperature gradients and the stratospheric polar vortex. In contrast, the TIL has only recently been recognized in the literature (Birner et al. 2002; Birner 2006), and the mechanisms that drive the TIL are still under investigation. Additionally, the TIL has not been examined in detail in the tropics. In this section, we examine the longitudinal structure of the TIL; in section 6, we examine the dominant forms of weekly and monthly variability that are associated with fluctuations in the magnitude of the TIL.

Figure 6 shows global, seasonal-mean maps of static stability averaged over a 1-km layer above the tropopause. Thus the panels capture the magnitude of the TIL as a function of latitude, longitude, and season. The dominant features in Fig. 6 are the meridional gradients in the strength of the TIL between tropical, middle, and polar latitudes. During all seasons, the magnitude of the TIL drops rapidly from the tropics to the midlatitudes. In general, the largest meridional gradients in the strength of the TIL are collocated with the flanks of the subtropical jet (Fig. 6, black contours). During the summer months, the TIL increases in strength from mid- to polar latitudes, with higher values of static stability found in the NH polar regions than in the SH polar regions. In fact, the magnitude of the TIL over the NH polar regions during

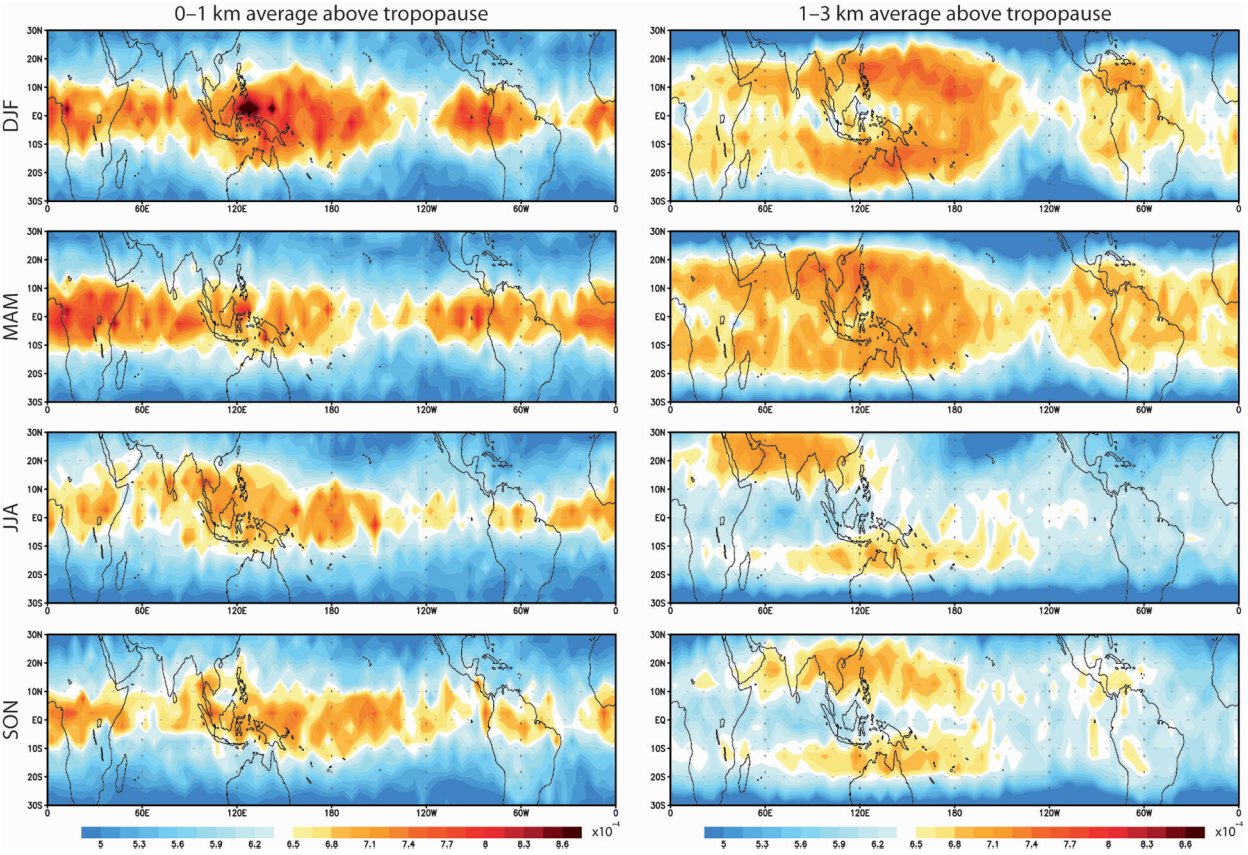

FIG. 7. As in Fig. 6, but focused on the tropics. The shading interval is 1.5×10^{-5} s^{-2}, with values below 5.0×10^{-4} s^{-2} not contoured. Note that the shading interval has been changed from Fig. 6 to emphasize the horizontal structure of the tropical features.

summer is comparable to that found in certain regions of the tropics (Fig. 6, top right). During the winter months, the extratropical TIL peaks at midlatitudes over the northeast Pacific and North Atlantic Oceans in the NH (Fig. 6, top left) and near New Zealand in the SH (Fig. 6, top right). The midlatitude features in Fig. 6 are evident throughout the 3-km layer above the tropopause, except for the North Atlantic feature, which is primarily limited to the ~1-km layer above the tropopause (not shown).

The zonal asymmetry of the TIL is most pronounced in the tropics. As highlighted in previous sections, the near-tropopause static stability in the tropics is characterized by two distinct features located at ~17 and ~19 km (~0–1 and ~1–3 km above the tropopause). Figure 7 shows the same results as those shown in Fig. 6, but it is focused on these tropical features. Note that the color scale in Fig. 7 is different than that used in Fig. 6 to accentuate the zonal structure of the results. As also evidenced in Figs. 1–3 and Fig. 5, the tropical static stability maximum located ~0–1 km above the tropopause is centered about the equator (left panels in Fig. 7), whereas the static stability maximum located ~1–3 km above the tropopause is centered between 10° and 20° latitude in both hemispheres (right panels in Fig. 7). The horizontal distribution of the 0–1-km static stability maximum is consistent with the structure of cold point tropopause temperatures (e.g., Highwood and Hoskins 1998; Randel et al. 2003; Gettelman and Birner 2007; Fueglistaler et al. 2009), and both the 0–1-km and 1–3-km maxima are reminiscent of the quasi-stationary equatorial Rossby and Kelvin wave responses to the diabatic heating associated with the climatological distribution of deep convection (e.g., Gill 1980; Highwood and Hoskins 1998; Dima and Wallace 2007; Fueglistaler et al. 2009). The results in Fig. 7 thus suggest that equatorial planetary waves likely play a central role in determining the unique horizontally and vertically varying structure of the tropical TIL. However, establishing the exact relationship between equatorial planetary waves and the static stability features in the tropical TIL requires a more detailed investigation and is beyond the scope of this study.

6. Stratospheric processes associated with variability in the TIL

In this section, we examine the processes that are associated with weekly and monthly variability in the strength

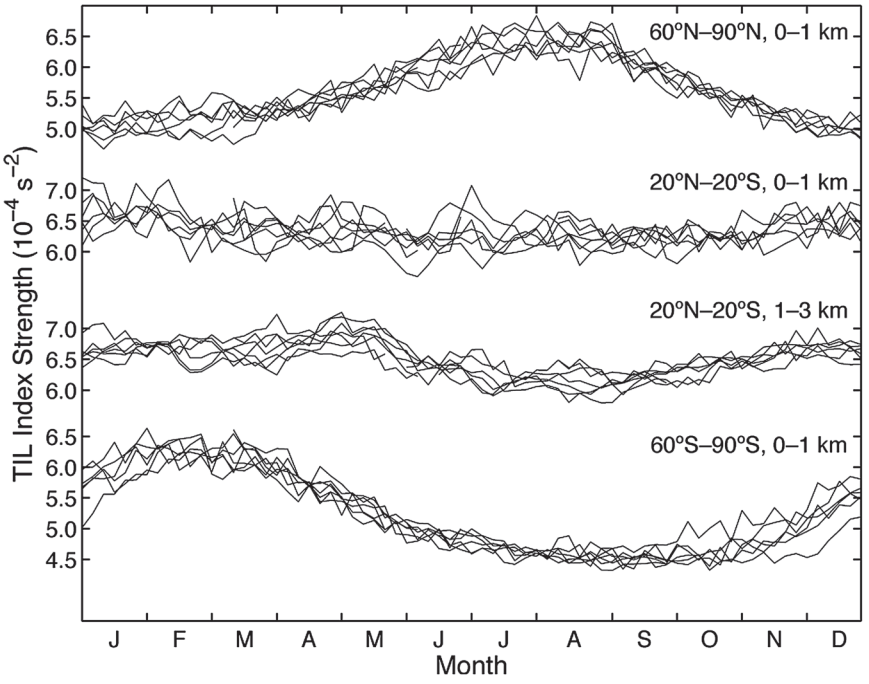

FIG. 8. TIL index time series averaged over 5-day periods and shown as a function of calendar day for the latitude bands and vertical ranges indicated (e.g., 0–1 km indicates the average of N^2 over the 0–1-km layer above the tropopause).

of the TIL at polar and tropical latitudes. To do this, we create an index of the strength of the TIL by averaging static stability over the depth of the TIL in each region. Because of the limited spatial and temporal sampling of the CHAMP data, the TIL index time series are based on 5-day averaged data only. We focus on polar and tropical latitudes since the TIL is most robust in those regions (Fig. 1, bottom).

Figure 8 shows plots of the TIL index time series as a function of calendar day based on the layer 0–1 km above the tropopause at polar latitudes and on the layers 0–1 and 1–3 km above the tropopause at tropical latitudes. Consistent with sections 3 and 4, the amplitude of the seasonal cycle of the TIL is largest in the polar regions, with peak values found during the summer seasons. Interestingly, the year-to-year variance in the polar TIL peaks during winter and summer in the NH and during spring and summer in the SH. The TIL exhibits a weak variance minimum during the NH fall season in the tropics.

The left panel in Fig. 9 shows the regressions of the 5-day-mean CHAMP static stability anomalies (averaged over 60°–90°N) upon wintertime values of the NH TIL index time series from Fig. 8. The index is standardized, and the seasonal cycle is removed prior to calculating the regression coefficients. As evidenced in Fig. 9 (left), positive anomalies in the strength of the NH polar TIL are associated with oppositely signed static stability anomalies that descend through the midstratosphere. The descending static stability anomalies in the midstratosphere are reminiscent of wave-driven variability in the NH stratospheric polar vortex. To isolate the anomalous static stability signature associated with stratospheric wave-driven variability, the right panel of Fig. 9 shows analogous regressions but for static stability regressed on the inverted 5-day-mean 10-hPa NAM index time series [the 10-hPa NAM index time series has been inverted (i.e., multiplied by −1) so that the signs of the regression coefficients correspond to a sudden stratospheric warming event]. Together, the results in the left and right panels of Fig. 9 reveal that the magnitude of the NH polar TIL is significantly linked to variability in the NH stratospheric polar vortex, with increased static stability in the vicinity of the TIL found during the period immediately following weakenings of the NH stratospheric polar vortex. Hence, whereas radiative processes may play a role in establishing the existence of the TIL (Randel et al. 2007b), dynamic variability in the NH polar stratosphere appears to contribute to intraseasonal variability in the strength of the NH winter polar TIL. We note that sudden stratospheric warmings are by construction associated with descending static stability anomalies along the lower edge of the stratospheric warming. However, it is less clear why they are also associated with a rapid

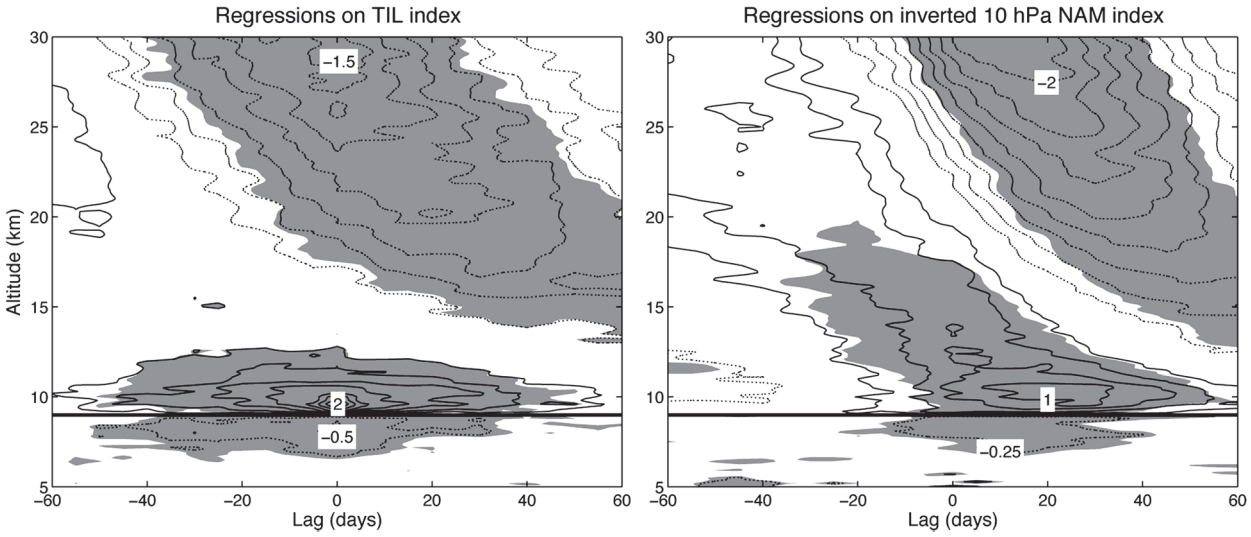

FIG. 9. Five-day-mean N^2 anomalies (averaged over 60°–90°N) regressed upon (left) wintertime values of the NH polar TIL index time series and (right) inverted (i.e., multiplied by −1) values of the 5-day-mean 10-hPa NAM index time series. The index time series lead (lag) the N^2 anomalies at positive (negative) lags. Positive contours are solid, negative contours are dotted, and the zero contour was omitted. The contour interval is 2.5×10^{-6} s^{-2}, and the contour labels are in units of 10^{-5} s^{-2}. Units are per standard deviation in (left) the TIL index time series and (right) the 10-hPa NAM index time series. The shading indicates regions that are 95% significant. The thick solid black line denotes the climatological November–April NH polar tropopause height.

sharpening of static stability immediately above the tropopause.

A similar relationship between the strength of the TIL and stratospheric dynamic variability is also evidenced in the SH polar regions. Because the SH stratospheric polar vortex is more quiescent than its NH counterpart, we rely on two case studies to hint at the importance of stratospheric dynamic variability on the SH polar TIL: the first case study is spring 2002, when the SH stratospheric polar vortex experienced an unprecedented sudden stratospheric warming (Shepherd et al. 2005); the second case study is spring 2006, when the SH polar vortex was anomalously strong. Figure 10 shows 5-day-mean time series of the static stability field (averaged over 60°–90°S) during SH spring for both of these cases. As in Fig. 4 (top row), the dashed line in each panel denotes the altitude at which the midlatitude jet is maximized. The anecdotal evidence in Fig. 10 clearly reveals that a narrow TIL formed following the sudden stratospheric warming in 2002 (Fig. 10, top) but not during the quiescent spring of 2006 (Fig. 10, bottom), despite the presence of large midstratospheric static stability values within the strong polar vortex of 2006. Additionally, note that the earlier seasonal breakdown of the SH stratospheric polar vortex in 2002 coincided with an anomalously strong TIL during early SH summer.

The results in Figs. 9 and 10 demonstrate marked covariability between stratospheric dynamical (i.e., wave driven) processes and intraseasonal variability in the strength of the polar TIL during the NH winter and SH spring seasons. The results thus suggest that stratospheric dynamical processes give rise to the peak in variance in the polar TIL during those seasons (Fig. 8). We have conducted similar analyses to examine the dynamical processes associated with the summertime variance maxima in the NH and SH polar TIL. However, we did not find any coherent dynamical structures in either the extratropical troposphere or the stratosphere that are clearly linked to variability in the strength of the polar TIL during the summer months (not shown).

In Fig. 11, we examine analogous relationships for the tropical TIL. The left panel shows the regressions of the 5-day-mean CHAMP static stability anomalies (averaged over 20°N–20°S) upon the 1–3-km tropical TIL index time series from Fig. 8. The index is standardized, and the seasonal cycle is removed prior to calculating the regression coefficients. Figure 11 (left) demonstrates that variability in static stability in the layer 1–3 km above the tropical tropopause is linked to descending static stability anomalies in the tropical midstratosphere that have a time scale reminiscent of that associated with the QBO. The sign of the results is such that positive static stability anomalies in the layer 1–3 km above the tropical tropopause are preceded by descending positive static stability anomalies in the tropical midstratosphere and vice versa. Interestingly, regressions based on the 0–1-km tropical TIL index time series (not shown) are only weakly linked to QBO-like static stability anomalies in the tropical midstratosphere.

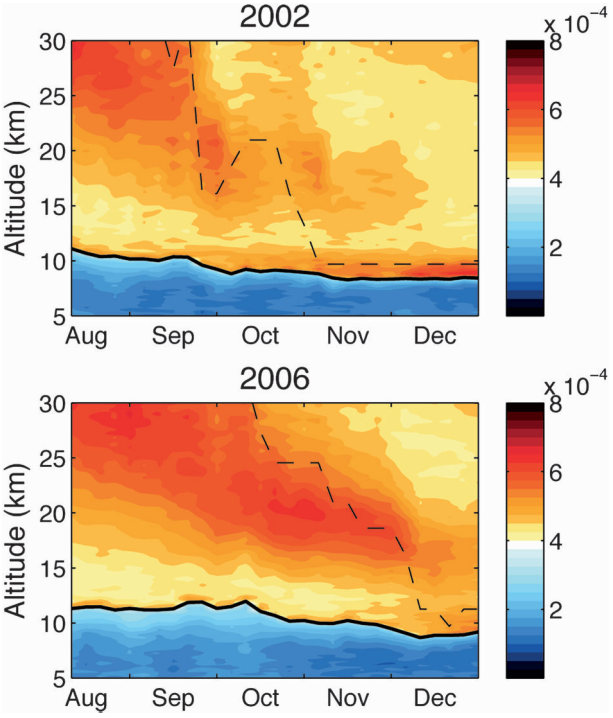

FIG. 10. Five-day-mean values of N^2 (averaged over 60°–90°S) for the period 9 Aug–31 Dec for (top) 2002 and (bottom) 2006. The shading interval is 2.5×10^{-5} s^{-2}. The thick solid black line denotes the 5-day-mean tropopause height in each plot. The dashed line denotes the altitude of the maximum 5-day-mean westerly zonal wind over the latitude band 50°–75°S. Note that the values of N^2 in this figure are not anomalies and thus include the seasonal cycle.

The above results suggest that variability in static stability in the layer 1–3 km above the tropical tropopause is linked to the QBO. To test this, we show in Fig. 11 (right) the results formed by regressing static stability onto the inverted 5-day-mean QBO index time series (recall that positive values of the inverted QBO index time series correspond to easterly zonal wind anomalies at 50 hPa). The descending static stability anomalies in the midstratosphere in Fig. 11 (right) correspond to the descending warm and cold temperature anomalies associated with the QBO. As the QBO decays toward the tropopause, the associated static stability anomalies disappear at ~20 km and then strengthen considerably in a narrow layer immediately above the tropopause.

Overall, the results in the left and right panels of Fig. 11 reveal that static stability anomalies in the layer 1–3 km above the tropical tropopause are significantly linked to QBO-driven variability in the tropical midstratosphere, with enhanced static stability near the tropical tropopause following the easterly phase of the QBO at 50 hPa. Past studies have noted that the easterly phase of the QBO at 50 hPa is associated with a cooler and higher tropical tropopause (e.g., Randel et al. 2000; Zhou et al. 2001), and Ratnam et al. (2006) has argued that the tropical tropopause is sharper during the easterly phase of the QBO in the lowermost stratosphere. The results shown here support these previous findings but also highlight the finescale nature of the linkages between the QBO and static stability in the lowermost tropical stratosphere: the QBO projects strongly onto static stability in the layer 1–3 km above the tropical tropopause but only weakly onto static stability in the layer 0–1 km above the tropical tropopause.

7. Summary and discussion

Static stability is a fundamental dynamical quantity, particularly for the propagation of atmospheric wave activity. Because static stability is proportional to the vertical gradient in temperature, temperature data with low vertical resolution inevitably smooth—or even fail to resolve—key aspects of the static stability field. For this reason, robust but finescale features in the global static stability field, including the shallow but pronounced tropopause inversion layer (TIL), are most clear in high vertical-resolution temperature datasets.

Previous papers have documented the existence of the TIL in the extratropics in high vertical resolution radiosonde data (Birner et al. 2002; Birner 2006; Bell and Geller 2008) and GPS radio occultation data (Randel et al. 2007b). They have also described the seasonal cycle of the TIL in the extratropics (Birner 2006; Randel et al. 2007b) and have provided an example of the TIL at a single tropical radiosonde station (Bell and Geller 2008). Here we extend previous studies of static stability by 1) documenting and examining the seasonally, zonally, and vertically varying structure of the static stability field in the stratosphere and upper troposphere on a global scale; 2) exploring the detailed structure of near-tropopause static stability in the tropics; and 3) examining the processes that are associated with week-to-week and month-to-month variability in the strength of the TIL.

In the long-term mean, the most pronounced feature in the global static stability field is the transition from low values in the troposphere to relatively high values in the stratosphere. In the extratropics, this pattern is accompanied by 1) a broad static stability maximum in the polar midstratosphere and 2) a shallow static stability maximum in the region immediately above the tropopause (Figs. 1 and 3). The large meridional gradients in static stability in the polar midstratosphere peak during the cold season (Figs. 3 and 4) and are in thermal wind balance with the stratospheric polar night jet (see the appendix). Hence, they are most pronounced in the SH

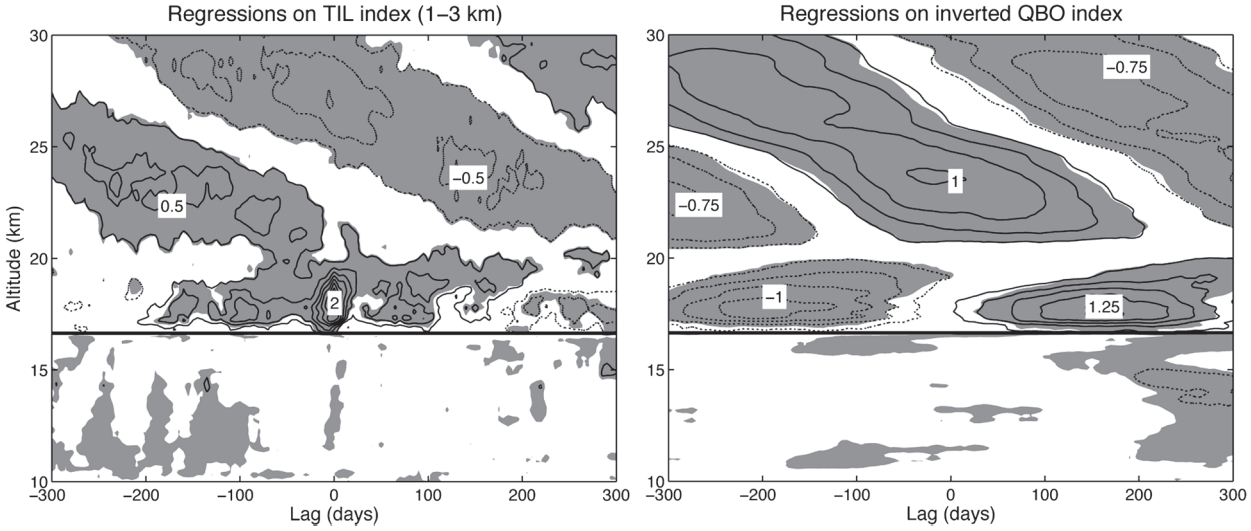

FIG. 11. As in Fig. 9, but for N^2 anomalies (averaged over 20°N–20°S) regressed upon (left) the 1–3-km tropical TIL index time series and (right) inverted (i.e., multiplied by −1) values of the QBO index time series. Positive values of the inverted QBO index time series denote easterly zonal wind anomalies at 50 hPa and vice versa. Units are per standard deviation in the (left) TIL index time series and (right) QBO index time series. The thick solid black line denotes the climatological tropical tropopause height.

during winter and descend through the polar stratosphere during spring as the stratospheric vortex breaks down (Figs. 3 and 4). The extratropical shallow static stability maximum reflects the signature of the TIL. As noted in Birner (2006) and Randel et al. (2007b), the TIL is deepest during the cold seasons at midlatitudes but is strongest during the warm seasons at polar latitudes.

In the tropics, the static stability field is marked by four primary features: 1) a static stability minimum in the upper troposphere, 2) a very shallow static stability maximum centered at the equator ~0–1 km above the tropopause, 3) paired static stability maxima in the lower stratosphere centered between 10° and 20° latitude in both hemispheres and located ~1–3 km above the tropopause, and 4) a broad region of high static stability values (much higher than those at comparable altitudes in the extratropics) that extend from the tropopause to ~25 km. The upper-tropospheric static stability minimum reflects the change in tropospheric lapse rate near the top of tropical convection (e.g., Gettelman and Forster 2002), and the broad region of high static stability values in the midstratosphere is consistent with radiative heating due to ozone (e.g., Kiehl and Solomon 1986; Andrews et al. 1987). But the unique vertically and horizontally varying structure of the static stability field in the vicinity of the tropical tropopause (i.e., the tropical TIL) has not been appreciated in previous literature [e.g., the recent review of the tropical tropopause layer by Fueglistaler et al. (2009) suggests that tropical static stability exhibits a single maximum near 70 hPa].

The finescale features in the static stability field in the vicinity of the tropical tropopause are robust. The static stability features centered ~0–1 and ~1–3 km above the tropical tropopause are reproducible in analyses based on the cold point tropopause (Fig. 2, right), they are consistent with the profile of static stability at Yap Island (located at 9°N) presented in Bell and Geller (2008), and they are evidenced in summertime averages of static stability based on high vertical resolution radiosonde data in the NH subtropics [cf. left edge of Fig. 7a (right) of Birner 2006]. Both features also exhibit physically meaningful horizontal structures. The lower feature bears resemblance to the pattern of cold point temperatures (e.g., Highwood and Hoskins 1998), and both the lower and upper features are reminiscent of the planetary wave response to the diabatic heating associated with the climatological distribution of tropical convection (e.g., Dima and Wallace 2007). Interestingly, the static stability feature located ~0–1 km above the tropical tropopause is stronger during the NH cold season at the equator, but it peaks during the summer season between 10° and 20° latitude in each hemisphere (Figs. 5 and 7). In contrast, the static stability feature located ~1–3 km above the tropical tropopause peaks during the NH cold season throughout the tropics (Figs. 5 and 7).

We also examined the processes that are associated with variability in the strength of the TIL at polar and tropical latitudes. In polar regions, the TIL exhibits enhanced variance during the winter and summer seasons in the NH and during the spring and summer

seasons in the SH. The variance maxima during NH winter and SH spring coincide with the ''active'' seasons for stratosphere–troposphere coupling, and during these seasons the strength of the TIL is coupled to stratospheric dynamic variability (i.e., periods following a weakening of the stratospheric polar vortex are marked by an anomalously strong TIL and vice versa). The variance maxima during the summer seasons are not linked to any obvious patterns of large-scale atmospheric variability. In the tropics, the amplitude of the static stability feature located ~1–3 km above the tropopause varies in association with the QBO, consistent with the juxtaposition of warm over cold temperature anomalies as the easterly phase of the QBO descends through the lowermost stratosphere. The narrow tropical TIL feature located ~0–1 km above the tropopause is not as clearly linked to the QBO.

There are two prevailing mechanisms thought to give rise to the TIL. Wirth (2003) and Wirth and Szabo (2007) argue that the TIL reflects the effects of sharp static stability gradients above tropospheric anticyclones. In contrast, Randel et al. (2007b) argue that the TIL is driven by radiative cooling due to water vapor near the tropopause superposed on radiative heating due to ozone in the lower stratosphere.

Our results suggest that a much broader range of processes govern the existence and variability of the TIL. The hypothesis proposed by Wirth (2003) applies only to extratropical latitudes, and the hypothesis proposed by Randel et al. (2007b) does not explain the unique structure of the TIL at tropical latitudes. The amplification of the polar TIL during sudden stratospheric warmings occurs on time scales shorter than the radiative time scale near the tropopause and suggests that the extratropical TIL is sensitive to stratospheric dynamics (see also Birner 2010). The horizontal structure of the tropical TIL suggests that it owes its existence at least in part to the planetary waves associated with tropical convection. Hence, the results presented here reveal that the TIL likely arises from a suite of radiative and dynamical processes operating at both stratospheric and tropospheric levels.

The structure and variability of the TIL documented here could be important in the context of stratosphere–troposphere dynamical coupling and chemical exchange. A much larger vertical gradient in static stability above the tropopause following a sudden stratospheric warming could affect the vertical propagation of tropospheric eddies, and thus could contribute to the changes in the tropospheric circulation observed in association with stratosphere–troposphere coupling (Baldwin and Dunkerton 2001). In fact, Simpson et al. (2009) have recently demonstrated the importance of the vertical distribution of static stability near the tropopause in determining the upper-tropospheric eddy momentum flux anomalies in an idealized general circulation model. The sharp gradients in static stability immediately above the tropical tropopause may also play a key role in the propagation of tropical waves and in the exchange of air between the tropical troposphere and the stratosphere. The importance of the narrow-scale features in near-tropopause static stability for stratosphere–troposphere coupling and exchange has yet to be determined.

Acknowledgments. We thank W. J. Randel for his helpful discussions of the results, and V. Wirth, L. M. Polvani, and an anonymous reviewer for their helpful comments on the manuscript. KMG and DWJT were supported by National Science Foundation Grant ATM-0613082.

APPENDIX

Relationships between Zonal-Mean Static Stability and Zonal-Mean Zonal Wind

In this appendix, we briefly review the relationships between zonal-mean static stability and the zonal-mean zonal wind. The zonal-mean zonal wind and potential temperature fields are related through the thermal wind relation, which can be approximated as

$$\frac{\partial u}{\partial z} \approx -\frac{g}{f\theta}\frac{\partial \theta}{\partial y}. \tag{A1}$$

Taking the vertical derivative of (A1) and substituting the definition of static stability (1), we obtain (A2) [cf. Eq. (5) of Birner 2006]:

$$\frac{\partial^2 u}{\partial z^2} = -\frac{1}{f}\frac{\partial}{\partial y}(N^2) \tag{A2}$$

Equation (A2) demonstrates that the meridional gradient of static stability is related to the vertical derivative of the vertical shear of the zonal wind, or equivalently to the vertical curvature of the zonal wind. For example, consider a westerly wind maximum where the vertical shear of the zonal wind is rapidly decreasing with height (i.e., changing from westerly to easterly). Equation (A2) mandates that a meridional gradient in static stability must exist across such a westerly wind maximum, with static stability increasing toward the pole. However, if the westerly wind maximum were barotropic or linearly

changing with height, no meridional gradient in static stability would be present.

REFERENCES

Andrews, D. G., J. R. Holton, and C. B. Leovy, 1987: *Middle Atmospheric Dynamics*. Academic Press, 489 pp.

Anthes, R. A., and Coauthors, 2008: The COSMIC/FORMOSAT-3 mission: Early results. *Bull. Amer. Meteor. Soc.,* **89,** 313–333.

Baldwin, M. P., and T. J. Dunkerton, 2001: Stratospheric harbingers of anomalous weather regimes. *Science,* **294,** 581–584.

Bell, S. W., and M. A. Geller, 2008: Tropopause inversion layer: Seasonal and latitudinal variations and representation in standard radiosonde data and global models. *J. Geophys. Res.,* **113,** D05109, doi:10.1029/2007JD009022.

Birner, T., 2006: Fine-scale structure of the extratropical tropopause region. *J. Geophys. Res.,* **111,** D04104, doi:10.1029/2005JD006301.

——, 2010: Residual circulation and tropopause structure. *J. Atmos. Sci.,* in press.

——, A. Dörnbrack, and U. Schumann, 2002: How sharp is the tropopause at midlatitudes? *Geophys. Res. Lett.,* **29,** 1700, doi:10.1029/2002GL015142.

——, D. Sankey, and T. G. Shepherd, 2006: The tropopause inversion layer in models and analyses. *Geophys. Res. Lett.,* **33,** L14804, doi:10.1029/2006GL026549.

Bretherton, C. S., M. Widmann, V. P. Dymnikov, J. M. Wallace, and I. Bladé, 1999: The effective number of spatial degrees of freedom of a time-varying field. *J. Climate,* **12,** 1990–2009.

Dima, I. M., and J. M. Wallace, 2007: Structure of the annual-mean equatorial planetary waves in the ERA-40 reanalyses. *J. Atmos. Sci.,* **64,** 2862–2880.

Frierson, D. M. W., 2008: Midlatitude static stability in simple and comprehensive general circulation models. *J. Atmos. Sci.,* **65,** 1049–1062.

——, I. M. Held, and P. Zurita-Gotor, 2006: A gray-radiation aquaplanet moist GCM. Part I: Static stability and eddy scale. *J. Atmos. Sci.,* **63,** 2548–2566.

Fueglistaler, S., A. E. Dessler, T. J. Dunkerton, I. Folkins, Q. Fu, and P. W. Mote, 2009: Tropical tropopause layer. *Rev. Geophys.,* **47,** RG1004, doi:10.1029/2008RG000267.

Gettelman, A., and P. M. Forster, 2002: A climatology of the tropical tropopause layer. *J. Meteor. Soc. Japan,* **80,** 911–924.

——, and T. Birner, 2007: Insights into tropical tropopause layer processes using global models. *J. Geophys. Res.,* **112,** D23104, doi:10.1029/2007JD008945.

Gill, A. E., 1980: Some simple solutions for heat-induced tropical circulation. *Quart. J. Roy. Meteor. Soc.,* **106,** 447–462.

Hajj, G. A., and Coauthors, 2004: CHAMP and SAC-C atmospheric occultation results and intercomparisons. *J. Geophys. Res.,* **109,** D06109, doi:10.1029/2003JD003909.

Hartmann, D. L., 1976: The structure of the stratosphere in the Southern Hemisphere during late winter 1973 as observed by satellite. *J. Atmos. Sci.,* **33,** 1141–1154.

Haynes, P., J. Scinocca, and M. Greenslade, 2001: Formation and maintenance of the extratropical tropopause by baroclinic eddies. *Geophys. Res. Lett.,* **28,** 4179–4182.

Held, I. M., 1982: On the height of the tropopause and the static stability of the troposphere. *J. Atmos. Sci.,* **39,** 412–417.

Highwood, E. J., and B. J. Hoskins, 1998: The tropical tropopause. *Quart. J. Roy. Meteor. Soc.,* **124,** 1579–1604.

Juckes, M. N., 2000: The static stability of the midlatitude troposphere: The relevance of moisture. *J. Atmos. Sci.,* **57,** 3050–3057.

Kalnay, E., and Coauthors, 1996: The NCEP/NCAR 40-Year Reanalysis Project. *Bull. Amer. Meteor. Soc.,* **77,** 437–471.

Kiehl, J. T., and S. Solomon, 1986: On the radiative balance of the stratosphere. *J. Atmos. Sci.,* **43,** 1525–1534.

Kistler, R., and Coauthors, 2001: The NCEP–NCAR 50-Year Reanalysis: Monthly means CD-ROM and documentation. *Bull. Amer. Meteor. Soc.,* **82,** 247–267.

Kursinski, E. R., and Coauthors, 1996: Initial results of radio occultation observations of earth's atmosphere using the global positioning system. *Science,* **271,** 1107–1110.

Lindzen, R. S., 1994: The effect of concentrated PV gradients on stationary waves. *J. Atmos. Sci.,* **51,** 3455–3466.

——, and G. Roe, 1997: The effect of concentrated PV gradients on stationary waves: Correction. *J. Atmos. Sci.,* **54,** 1815–1818.

Peixoto, J. P., and A. H. Oort, 1992: *Physics of Climate*. American Institute of Physics, 520 pp.

Randel, W. J., F. Wu, and D. J. Gaffen, 2000: Interannual variability of the tropical tropopause derived from radiosonde data and NCEP reanalysis. *J. Geophys. Res.,* **105** (D12), 15 509–15 523.

——, ——, and W. R. Ríos, 2003: Thermal variability of the tropical tropopause region derived from GPS/MET observations. *J. Geophys. Res.,* **108,** 4024, doi:10.1029/2002JD002595.

——, M. Park, F. Wu, and N. Livesey, 2007a: A large annual cycle in ozone above the tropical tropopause linked to the Brewer–Dobson circulation. *J. Atmos. Sci.,* **64,** 4479–4488.

——, F. Wu, and P. Forster, 2007b: The extratropical tropopause inversion layer: Global observations with GPS data, and a radiative forcing mechanism. *J. Atmos. Sci.,* **64,** 4489–4496.

Ratnam, M. V., T. Tsuda, T. Kozu, and S. Mori, 2006: Long-term behavior of the Kelvin waves revealed by CHAMP/GPS RO measurements and their effects on the tropopause structure. *Ann. Geophys.,* **24,** 1355–1366.

Ryu, J.-H., S. Lee, and S.-W. Son, 2008: Vertically propagating Kelvin waves and tropical tropopause variability. *J. Atmos. Sci.,* **65,** 1817–1837.

Schneider, T., 2004: The tropopause and the thermal stratification in the extratropics of a dry atmosphere. *J. Atmos. Sci.,* **61,** 1317–1340.

Seidel, D. J., and W. J. Randel, 2007: Recent widening of the tropical belt: Evidence from tropopause observations. *J. Geophys. Res.,* **112,** D20113, doi:10.1029/2007JD008861.

Shepherd, T., R. A. Plumb, and S. C. Wofsy, 2005: Preface. *J. Atmos. Sci.,* **62,** 565–566.

Simpson, I. R., M. Blackburn, and J. D. Haigh, 2009: The role of eddies in driving the tropospheric response to stratospheric heating perturbations. *J. Atmos. Sci.,* **66,** 1347–1365.

Son, S.-W., and L. M. Polvani, 2007: Dynamical formation of an extra-tropical tropopause inversion layer in a relatively simple general circulation model. *Geophys. Res. Lett.,* **34,** L17806, doi:10.1029/2007GL030564.

——, S. Lee, and S. B. Feldstein, 2007: Intraseasonal variability of the zonal-mean extratropical tropopause height. *J. Atmos. Sci.,* **64,** 608–620.

Tomikawa, Y., Y. Nishimura, and T. Yamanouchi, 2009: Characteristics of tropopause and tropopause inversion layer in the polar region. *Sci. Online Lett. Atmos.,* **5,** 141–144.

Wickert, J., and Coauthors, 2001: Atmosphere sounding by GPS radio occultation: First results from CHAMP. *Geophys. Res. Lett.,* **28,** 3263–3266.

Wirth, V., 2003: Static stability in the extratropical tropopause region. *J. Atmos. Sci.,* **60,** 1395–1409.

——, and T. Szabo, 2007: Sharpness of the extratropical tropopause in baroclinic life cycle experiments. *Geophys. Res. Lett.,* **34,** L02809, doi:10.1029/2006GL028369.

WMO, 1957: Meteorology – A three-dimensional science. *WMO Bull.,* **6,** 134–138.

Yulaeva, E., J. R. Holton, and J. M. Wallace, 1994: On the cause of the annual cycle in tropical lower-stratospheric temperatures. *J. Atmos. Sci.,* **51,** 169–174.

Zängl, G., and K. P. Hoinka, 2001: The tropopause in the polar regions. *J. Climate,* **14,** 3117–3139.

——, and V. Wirth, 2002: Synoptic-scale variability of the polar and subpolar tropopause: Data analysis and idealized PV inversions. *Quart. J. Roy. Meteor. Soc.,* **128,** 2301–2315.

Zhou, X. L., M. A. Geller, and M. H. Zhang, 2001: Tropical cold point tropopause characteristics derived from ECMWF reanalysis and soundings. *J. Climate,* **14,** 1823–1838.